

A Comparison of the Weakly Nonlinear Instability of Westerly and Easterly Jets in a Two-Layer Beta-Plane Model

STEVEN B. FELDSTEIN

Department of Earth and Atmospheric Science, York University, North York, Ontario, Canada

(Manuscript received 8 May 1990, in final form 4 February 1991)

ABSTRACT

The nonlinear evolution of disturbances that emanate from unstable westerly and easterly jet profiles is examined with a two-layer quasi-geostrophic β -plane channel model. Significant differences arise between the solutions for westerly and easterly jets. For unstable narrow (width less than the deformation radius) westerly jets, the disturbance undergoes a sequence of life cycles characterized by barotropic growth and barotropic decay. Unstable easterly jets also give rise to a series of life cycles in which the disturbance grows and decays in a combined baroclinic/barotropic manner. In each of these cases, the disturbance structure remains close to its unstable normal mode form throughout the life cycle. This contrasts with earlier results of Feldstein and Held who find that disturbances emanating from unstable wide (width greater than the deformation radius) westerly jets undergo a change in meridional structure, enhanced lateral radiation, and a single life cycle consisting of baroclinic growth followed by barotropic decay.

The wave propagation characteristics of the westerly and easterly jets are examined in the context of linear WKB theory. It is found that the modes growing in the narrow westerly and easterly jets are reflected at turning latitudes. On the other hand, the modes of the unstable wide westerly jet are completely absorbed at critical latitudes. These properties at the bounding latitudes are used to explain differences in the life cycles.

The life cycles for westerly and easterly jets are also examined with a forced dissipative model. For both narrow westerly and easterly jets, the disturbance always evolves to a steady state. This contrasts with the multiple life cycle solutions of the wide westerly jet. Finally, the results in this study are related to the nonlinear instability of various jets in the atmosphere.

1. Introduction

The two-layer quasi-geostrophic model has been extensively used to study a wide diversity of problems in large-scale atmospheric dynamics. Even though its vertical resolution is crude, the two-layer quasi-geostrophic model has yielded much insight into many fundamental properties of large-scale atmospheric flows. One issue of major importance to the atmospheric general circulation is nonlinear baroclinic instability. Through this process, evolving synoptic-scale baroclinic waves transport large quantities of heat and momentum. Several different two-layer quasi-geostrophic models have been particularly successful in elucidating many properties of the growth and decay of baroclinic waves. These include the weakly nonlinear studies of Pedlosky (1970, 1971, 1980, 1981) and Loesch (1974a,b), the low-order spectral models of Boville (1980, 1981, 1982), Mak (1985), and Cai and Mak (1986), and the high resolution gridpoint model solutions of Feldstein and Held (1989, FH hereafter). With the exception of FH, the above models all restrict

the initial zonal flow to a constant value in each layer. Thus, the barotropic conversions between the waves and the zonally averaged flow are initially suppressed and remain small throughout the life cycle. As a result, the growth and decay of the waves is almost entirely baroclinic. In FH, upper-layer meridional shear is included in the zonal flow. When the meridional shear is strong enough to produce a critical latitude, the waves undergo a life cycle of baroclinic growth followed by barotropic decay. This life cycle closely resembles those of the multilevel spherical primitive equation model experiments of Simmons and Hoskins (1978, 1980) and the observational studies of Randel and Stanford (1985a,b) for baroclinic waves in the Southern Hemisphere. Thus, the results of FH imply that the two-layer quasi-geostrophic model is indeed capable of reproducing the dominant features of baroclinic wave evolution in the atmosphere.

Motivated by its success in explaining many key properties of baroclinic wave evolution, I have used the model in FH to compare the nonlinear instability of westerly and easterly jets. In order to study the temporal evolution of the evolving waves in as simple a context as possible, the supercriticality of the initial zonal jet is weak and the wave is restricted to one zonal wavenumber. Westerly and easterly jets in the equal-

Corresponding author address: Dr. Steven B. Feldstein, Dept. of Earth and Atmospheric Science, York University, 4700 Keele Street, North York, Ontario M3J 1P3, Canada.

depth, two-layer quasi-geostrophic model do not have the same symmetrical linear instability properties as is the case when the zonal flow is uniform in each layer (see Pedlosky 1987). The source of this asymmetry is that the horizontal curvature $\partial^2 U/\partial y^2$ reverses sign with the change in direction of the jet, whereas the planetary vorticity gradient β does not. As an example, consider the following zonal jet profile for the two-layer model [the standard nondimensional notation of Pedlosky (1987) is used]:

$$U_1(y) = U_0 \operatorname{sech}^2(y - y_0)/\sigma; \quad U_2(y) = 0, \quad (1)$$

where σ is a positive constant that measures the width of the jet, U_0 can be positive or negative, y is latitude, y_0 is a constant, and the magnitude of U_0 is sufficiently large so that (1) is unstable. The meridional potential vorticity gradient for a jet of this form is

$$\begin{aligned} \partial Q_1/\partial y &= \beta - \partial^2 U_1/\partial y^2 + \frac{1}{2} U_1; \\ \partial Q_2/\partial y &= \beta - \frac{1}{2} U_1, \end{aligned} \quad (2)$$

where Q_n is the potential vorticity, $n = 1$ denotes the upper layer and $n = 2$ the lower layer, and the Rossby radius of deformation is chosen as the horizontal length scale. If $U_0 > 0$, unstable regions (the region where $\partial Q_n/\partial y$ is negative) can occur in two narrow latitudinal bands (if σ is sufficiently small) at the wings of the jet in the upper layer and at the center of the lower layer. Horizontal curvature of the zonal flow leads to the formation of the upper-layer unstable regions, whereas vertical shear of the zonal flow generates the lower layer unstable region. This suggests that the westerly jet can be barotropically and/or baroclinically unstable if the horizontal curvature and/or vertical shear is strong enough. On the other hand, if $U_0 < 0$, the unstable region is confined to the middle of the upper layer. In this case, the combined effects of both horizontal curvature and vertical shear reinforce each other toward the formation of the unstable region. This suggests that the easterly jet is both baroclinically and barotropically unstable.

The above asymmetries in the linear stability properties of westerly and easterly jets are not confined just to the two-layer quasi-geostrophic model. For example, consider the following zonal wind profile:

$$U(y, z) = U_0 z \operatorname{sech}^2(y - y_0)/\sigma, \quad (3)$$

where $z \geq 0$. In general, for a zonal wind that is continuous in y and z ,

$$\begin{aligned} \partial Q/\partial y &= \beta - \partial^2 U/\partial y^2 - (1/S)\partial^2 U/\partial z^2 \\ &\quad - (1/\rho_s)\partial(\rho_s/S)/\partial z \partial U/\partial z, \end{aligned} \quad (4)$$

where $\rho_s(z)$ is a rest state density and S is a stratification parameter (see Pedlosky 1987). For the following argument, it is assumed that $\partial(\rho_s/S)/\partial z < 0$, which is

typically the case in the troposphere. If $U_0 > 0$, unstable regions can occur both at the ground due to the boundary temperature gradient [$\partial Q/\partial y$ has a negative delta function structure at the lower boundary when the surface meridional temperature gradient is negative (Bretherton 1966)] and in the interior of the fluid at the wings of the jet. When $U_0 < 0$, there is a single unstable region that is confined to a latitudinal band that is symmetric about the center of the jet. This unstable region is no longer on the lower boundary and is found only within the interior of the fluid. In addition, any $U_0 > 0$ satisfies the Charney–Stern necessary condition for instability, whereas if $U_0 < 0$, this criterion is met only if the vertical shear is sufficiently large.

In a sense, we can make an analogy between the lower boundary (interior of the fluid) of the continuous model and the lower (upper) layer of the two-layer quasi-geostrophic model. This is because of the agreement in the sign of $\partial Q_n/\partial y$ between analogous regions. In the case of the easterly jet, the argument for this analogy is stronger, as both models have a minimum vertical shear that is necessary for instability. Thus, even though we are only going to examine the nonlinear evolution of baroclinic waves within the context of the two-layer quasi-geostrophic model, it would not be surprising if similar behavior is observed in a more realistic continuous model.

In addition to being an interesting theoretical problem, an examination of the nonlinear instability of both easterly jets and very narrow (when $\partial^2 U/\partial y^2$ is sufficiently strong to cause a sign change in $\partial Q/\partial y$) westerly jets is of geophysical relevance. For example, several modeling studies have indicated that the African easterly jet is barotropically unstable (Rennick 1976; Simmons 1977; Mass 1979; Kwon 1989). In the most recent of these studies, Kwon (1989) used a moist quasi-geostrophic model to show that the combined barotropic/baroclinic instability of realistic African jets can generate disturbances that resemble African easterly waves. Another easterly jet is seen in the summer upper troposphere south of the Tibetan plateau. The linear stability of this jet has been examined by Mishra and Tandon (1983) with a multilevel quasi-geostrophic model. As with the African jet, they find that this jet can be both barotropically and baroclinically unstable. In the mesosphere, strong easterly jets also occur during the summer. Pfister (1985) and Plumb (1983), using idealized linear quasi-geostrophic models, showed that the summer mesosphere easterly jet may indeed be baroclinically and/or barotropically unstable. They both speculated that the observed traveling waves in the summer mesosphere arise from this instability. In addition, narrow westerly jets occur regularly in the winter stratosphere of both hemispheres. The linear stability of these jets was studied by Hartmann (1983), who showed that regions with negative meridional potential vorticity gradients occur on the flanks of the westerly jet in the Southern Hemisphere winter strato-

sphere. This suggestion of in situ barotropic instability in the winter stratosphere has been tested with idealized quasi-geostrophic linear barotropic models by Manney et al. (1988), Hartmann (1983), and Pfister (1979). Each of these studies finds barotropically unstable modes that are of planetary scale and have periods that are remarkably similar to those observed in the winter stratosphere of both hemispheres.

The linear stability properties of westerly and easterly jets are discussed in section 3. The life cycle solutions for the disturbances that grow from the unstable jets are examined in section 4. Forcing and dissipation are added in section 5.

2. Model description

The same two-layer quasi-geostrophic model as in FH is used. When the streamfunction ψ and the potential vorticity q are separated into a zonal mean part and a disturbance,

$$\begin{aligned}\psi_n(x, y, t) &= \Psi_n(y, t) + \psi'_n(x, y, t) \\ q_n(x, y, t) &= Q_n(y, t) + q'_n(x, y, t),\end{aligned}\quad (5)$$

where ψ_n and q_n are related by

$$q_n = \nabla^2 \psi_n + \beta y + (-1)^n (\psi_1 - \psi_2)/2. \quad (6)$$

The dimensionless disturbance vorticity equation becomes

$$\partial q'_n / \partial t + U_n \partial q'_n / \partial x + v'_n \partial Q_n / \partial y = -\nu \nabla^6 \psi'_n, \quad (7)$$

and the dimensionless zonal mean potential vorticity equation has the form

$$\partial Q_n / \partial t = -\partial(\overline{v'_n q'_n}) / \partial y - \nu \nabla^6 \Psi_n. \quad (8)$$

The biharmonic diffusion in (7) and (8) is used to parameterize the enstrophy cascade to small scales. The overbar in (8) denotes a zonal average.

Different initial zonal flows of the form

$$U_1(y, 0) = U(y); \quad U_2(y, 0) = 0 \quad (9)$$

will be employed, where $U(y)$ has been scaled so that it has a magnitude of 1.0 in the center of the channel. In this model, the fluid is bounded by rigid walls at $y = 0, W$. In order that the perturbation meridional velocity vanishes at the walls, the conditions

$$\partial \psi'_n / \partial x = 0 \quad \text{at } y = 0, W \quad (10)$$

and

$$\partial U_n / \partial t = -\nu \partial^4 U_n / \partial y^4 \quad \text{at } y = 0, W \quad (11)$$

are required. Equations (10) and (11) can be satisfied if we set

$$\psi'_n(x, 0, t) = \psi'_n(x, W, t) = 0$$

$$U_n(0, t) = U_n(0, 0) \quad \text{and} \quad U_n(W, t) = U_n(W, 0). \quad (12)$$

Because of the presence of the higher order diffusion term, we must also include an additional four boundary conditions (see FH).

The numerical procedure adopted in this model is also the same as in FH. Briefly, the model equations are integrated with the leapfrog scheme and the computational mode is suppressed by periodically restarting the integration. There are equally spaced grid points in the meridional direction and a single zonal wavenumber in the zonal direction.

3. Linear theory

As stated in the Introduction, we will be investigating the life cycles of disturbances that emanate from a variety of different westerly and easterly jet profiles. Before looking at the nonlinear evolution of these disturbances, it will be beneficial to examine the linear stability properties of the same jet profiles that will be used in the life cycle calculations. These jet profiles have the form

$$U_1(y) = \pm \text{sech}^2(y - y_0) / \sigma; \quad U_2(y) = 0, \quad (13)$$

where $y_0 = 0.5W$ and σ is the jet width. For all calculations W will be sufficiently large so that the upper-layer zonal wind goes to zero before the channel wall. In addition, the horizontal diffusion coefficient ν is set to zero, as it is found irrelevant to the linear stability analysis.

Our aim is to determine both the maximum value of β below which instability can occur, β_c , as well as the corresponding zonal wavenumber k_c . This is accomplished by numerically integrating (7) with one zonal wavenumber and keeping all zonal mean quantities fixed until the disturbance attains its normal mode form with its distinct phase speed and growth rate. In all linear stability calculations, the disturbance, which is the fastest growing normal mode, is always symmetric about the center of the jet. When linear stability analyses are performed on flows such as (13), a resolution problem occurs in the limit of the supercriticality approaching zero. This is because, as we will see, the unstable disturbances have a critical latitude [the latitude y_c where $U_1(y_c) - c_r = 0$] somewhere in $0 \leq y \leq W$. Since the critical latitude width is proportional to the growth rate of the disturbance [the critical latitude width $L_c \propto c_i (\partial U_1 / \partial y)^{-1}$ at y_c], infinitesimally fine resolution is required in the limit of vanishing supercriticality. In order to overcome this problem, disturbances with a growth rate $\omega_i = 0.02$ will be regarded as marginally stable. (It should be emphasized that disturbances with $0 < \omega_i < 0.02$ and $\beta < \beta_c$ are still unstable, and the term marginal stability is being used to denote unstable disturbances with growth $\omega_i = 0.02$. This is done in order to minimize the computational expense of generating the "true" $\omega_i = 0$ marginal stability curve.) At this value of ω_i , it is found that linear stability analyses can be performed accurately within

a reasonable amount of time using a time step of 0.01 with 200 grid points in the meridional direction. Thus, the approach to be used in the linear stability analysis is to gradually increase β until a growth rate of $\omega_i = 0.02$ is achieved. It is this value of β that will be regarded as β_c .

a. Westerly jet

The marginal stability curve for the $\sigma = 1.0$ westerly jet with $W = 7.5$ is shown in Fig. 1. The zonal wind U_n and the meridional potential vorticity gradient $\partial Q_n / \partial y$ for the $\sigma = 1.0$ jet at $\beta = 0.42$ are illustrated in Fig. 2. As stated above, the curve of marginal stability is chosen to correspond to $\omega_i = 0.02$. The precise value of β_c is determined by linear interpolation of ω_i between two values of β with growth rates greater than and less than 0.02. The results of this linear stability analysis show that the marginally stable β has maximum values at $\beta_c = 0.361$ and 0.433 at zonal wavenumbers $k_c = 0.84$ and 1.42 , respectively. A determination of the linearly unstable energetics for a range of values of k indicates that there is 1) a set of baroclinically unstable modes associated with the small wavenumber maxima at $\beta_c = 0.361$ and 2) a set of barotropically unstable modes associated with the large wavenumber maxima at $\beta_c = 0.433$.

Next, we examine the linear instability of the westerly jet version of (13) with $\sigma = 0.75, 3.0$, and 24.0 . In relation to the atmosphere, the first value of σ corresponds to a narrow jet, the second to a typical jet, and the third to an unrealistically wide jet. As we will see, for the $\sigma = 1.0$ jet and the above three jets, the nonlinear life cycles are fundamentally different. For these three jets, the linear stability calculations find the following

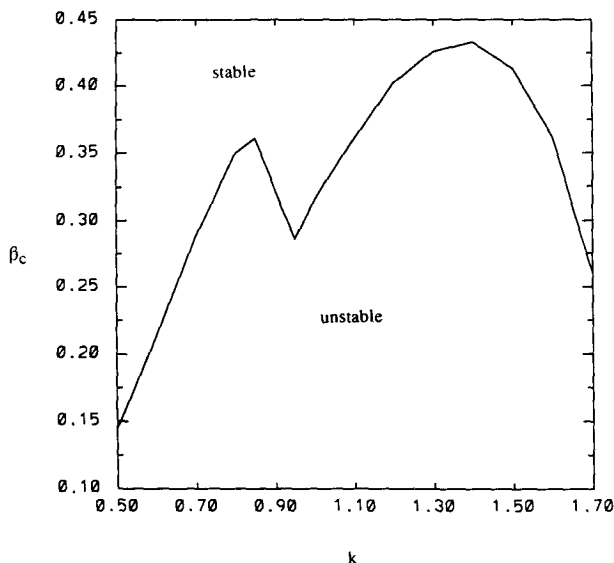


FIG. 1. β_c as a function of zonal wavenumber k for the $\sigma = 1.0$ westerly jet.

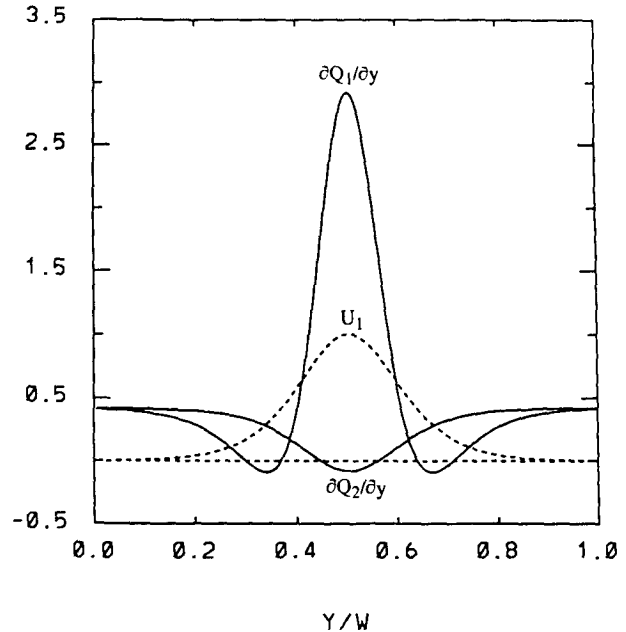


FIG. 2. The initial upper-layer zonal wind U_1 and meridional potential vorticity gradient $\partial Q_n / \partial y$ for the $\sigma = 1.0$ westerly jet with $\beta = 0.42$.

pairs of (β_c, k_c) : $\sigma = 24.0$ (0.488, 0.82) for $W = 150.0$; $\sigma = 3.0$ (0.42, 0.82) for $W = 30.0$; and $\sigma = 0.75$ (0.93, 1.72) for $W = 7.5$. For the $\sigma = 24.0$ and 3.0 jets, the unstable region is confined to the lower layer. The source of the instability is the vertical shear of the zonal wind. As σ is further reduced (i.e., when $\sigma = 1.0$), the jet becomes narrower and the increase in the horizontal curvature at the wings of the jet leads to the formation of a second unstable region in the upper layer. Finally, when the jet is narrow enough (as in the $\sigma = 0.75$ case) so that the horizontal curvature dominates the vertical shear, the unstable region is confined entirely to the upper layer. An inspection of the sign of $\partial Q_n / \partial y$ would suggest that the $\sigma = 3.0$ and 24.0 jets are baroclinically unstable, the $\sigma = 1$ jet is both baroclinically and barotropically unstable, and the $\sigma = 0.75$ jet is barotropically unstable. This property is indeed verified by a linear stability analysis. Calculations for other values of σ verify the general property that there are two fundamentally different types of unstable modes. When the jet width σ is significantly larger (smaller) than the Rossby radius of deformation, the instability is baroclinic (barotropic).

In order to summarize the structure of the baroclinically and barotropically unstable modes, we consider two unstable $\sigma = 1.0$ modes with the (β, k) pairs (0.42, 0.84) and (0.36, 1.10), respectively (see Fig. 3). The baroclinically unstable mode has a growth rate $\omega_i = 0.005$, whereas the barotropically unstable mode has a larger growth rate of $\omega_i = 0.02$. A smaller growth rate is chosen for the baroclinically unstable mode in order to more accurately locate the critical latitude. For the

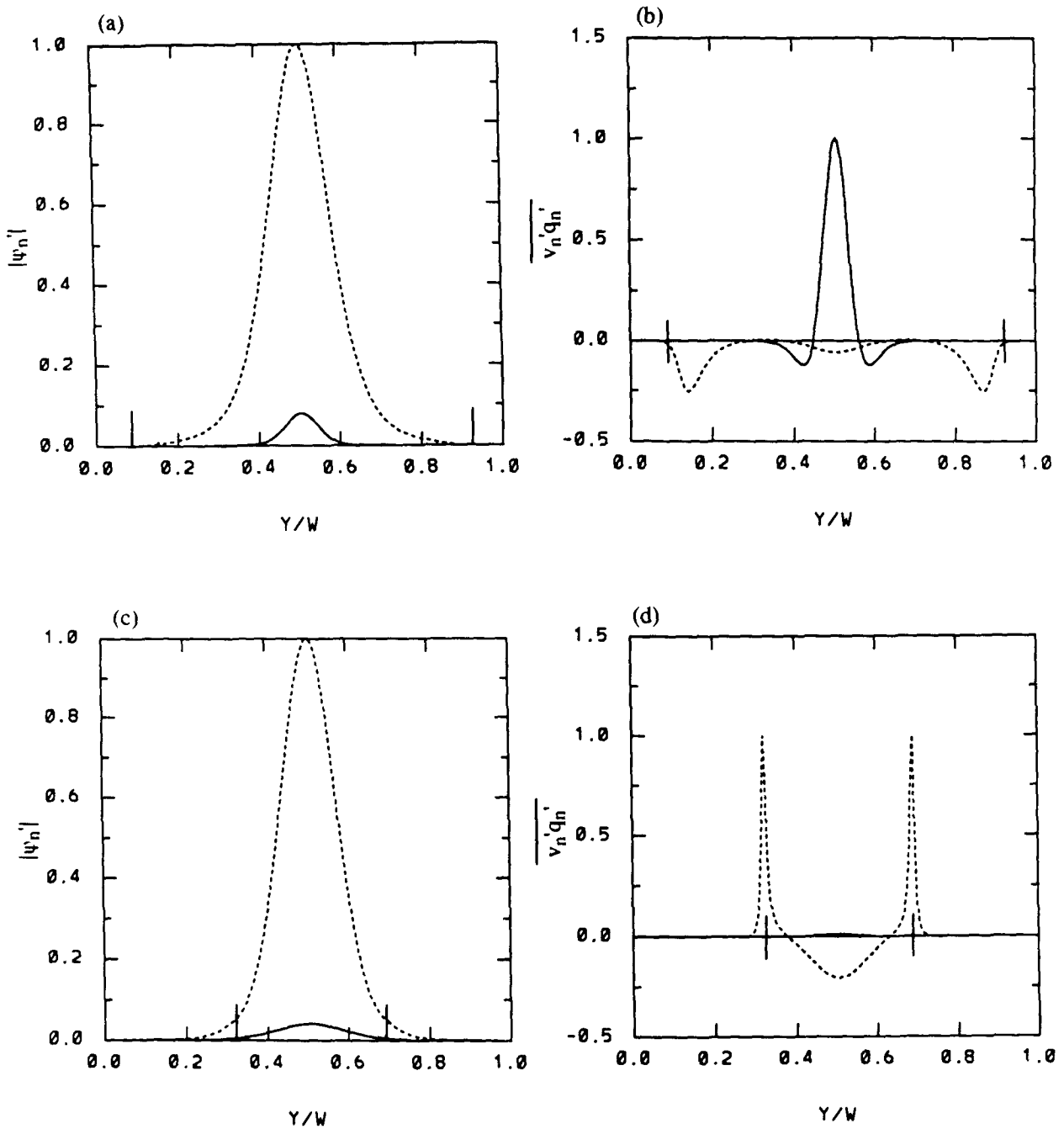


FIG. 3. (a) The magnitude of the streamfunction for the $\sigma = 1.0$ westerly jet baroclinically unstable mode with $\beta = 0.42$ and $k = 0.84$; and (b) potential vorticity flux for the baroclinically unstable mode. (c) The magnitude of the streamfunction for the $\sigma = 1.0$ westerly jet barotropically unstable mode with $\beta = 0.361$ and $k = 1.10$; and (d) potential vorticity flux for the barotropically unstable mode. The solid line corresponds to the lower layer and the dashed line to the upper layer. The streamfunctions and potential vorticity fluxes are normalized by their maximum value. The short vertical lines denote the location of the linear critical latitude.

baroclinically unstable mode, the amplitude of the upper layer streamfunction and potential vorticity flux are essentially zero at and beyond the linear critical latitude. On the other hand, for the barotropically unstable mode, the streamfunction amplitude and potential vorticity flux go to zero at a latitude beyond the

critical latitude. In fact, as is seen in Fig. 3d, the upper layer potential vorticity flux actually attains its maximum value at the critical latitude.

In order to examine the wave propagation characteristics of the unstable modes, a WKB solution is obtained in the following manner. When solutions to the

linear version of (7) are assumed to have the form $\psi'_n(x, y, t) = \psi_n(y)e^{-ikct}$, where k is the zonal wavenumber and the complex phase speed $c = c_r + ic_i$, (7) takes on the form

$$\begin{aligned} d^2\psi_1/dy^2 + a_{11}\psi_1 + a_{12}\psi_2 &= 0; \\ d^2\psi_2/dy^2 + a_{21}\psi_1 + a_{22}\psi_2 &= 0, \end{aligned} \quad (14)$$

where

$$\begin{aligned} a_{11} &= (\partial Q_1/\partial y)/(U_1 - c) - (k^2 + 1/2); \\ a_{22} &= (\partial Q_2/\partial y)/(U_2 - c) - (k^2 + 1/2); \\ a_{12} &= a_{21} = 1/2. \end{aligned} \quad (15)$$

The coefficients a_{ij} are functions of y and depend on parameters such as β_c , k , and c . As the focus of this study is on weakly supercritical flows (i.e., in the limit as c_i approaches zero), for our WKB solution to (14), we will take c to be real (i.e., the small c_i will be neglected). This implies that the a_{ij} are real. In order to formulate a WKB solution, a small parameter must be specified. For this particular problem we define the small parameter $\epsilon^{-2} = |\max(a_{ij}(y))| \gg 1$, where $\max(f(y))$ denotes the maximum value of $f(y)$ within $0 \leq y \leq W$ except in the vicinity of $U(y) - c = 0$. After defining $A_{ij} = a_{ij}\epsilon^2$, (14) becomes

$$\begin{aligned} \epsilon^2 d^2\psi_1/dy^2 + A_{11}\psi_1 + A_{12}\psi_2 &= 0; \\ \epsilon^2 d^2\psi_2/dy^2 + A_{21}\psi_1 + A_{22}\psi_2 &= 0. \end{aligned} \quad (16)$$

This system admits solutions of the form

$$\begin{aligned} \psi_n(y) &= \alpha_n \exp(i/\epsilon \sum_{n=0}^{\infty} \epsilon^n S_n(y)) \\ &= \alpha_n \exp(iS(y)/\epsilon) \end{aligned} \quad (17)$$

where $S(y) = \sum_{n=0}^{\infty} \epsilon^n S_n(y)$. After substituting (17) into (16), the $O(1)$ system of equations is

$$\begin{aligned} -\alpha_1 (dS_0/dy)^2 + A_{11}\alpha_1 + A_{12}\alpha_2 &= 0; \\ -\alpha_2 (dS_0/dy)^2 + A_{21}\alpha_1 + A_{22}\alpha_2 &= 0. \end{aligned} \quad (18)$$

This system of equations admits nontrivial solutions for α_1 and α_2 only if the determinant of the coefficient matrix vanishes. If we define τ as an eigenvalue of the matrix $\{A_{ij}\}$, solutions to (18) must satisfy $(dS_0/dy)^2 = \tau$, or if we define μ to be an eigenvalue of the matrix $\{a_{ij}\}$, we obtain $(dS_0/dy)^2 = \mu\epsilon^2$. Solving for S_0 implies that

$$S_0 = \epsilon \int \mu^{1/2} dy. \quad (19)$$

The $O(\epsilon)$ system of equations leads to the presence of just one equation

$$2(dS_0/dy)(dS_1/dy) + id^2S_0/dy^2 = 0, \quad (20)$$

which, after substituting for S_0 in (20), gives $S_1 = -i$

$\ln\mu^{-1/4}$. Last, we substitute for S_0 and S_1 in (17) to obtain our $O(\epsilon)$ WKB solution to (14), which is

$$\begin{aligned} \psi_n(y) &= \alpha_n \exp\left[i/\epsilon \left(\epsilon \int \mu^{1/2} dy - \epsilon i \ln\mu^{-1/4} \right)\right] \\ &= \alpha_n \mu^{-1/4} \exp\left(i \int \mu^{1/2} dy\right). \end{aligned} \quad (21)$$

Also, at this stage, it is important to emphasize that this WKB approach is not valid in the vicinity of turning and critical latitudes. Nevertheless, the WKB solution is valid away from these regions. Our primary aim is not a precise determination of the local meridional wavenumber or wave amplitude but it is to specify regions of propagation and evanescence. It is straightforward to show that at any $0 \leq y \leq W$ the matrix $\{a_{ij}\}$ has two real eigenvalues. Since the local meridional wavenumber is equal to $\mu^{1/2}$, if μ is positive (negative) the disturbance is characterized by propagation (evanescence). Calculations were done to determine $\mu(y)$ for both the $\sigma = 1.0$ baroclinically and barotropically unstable modes. For easier viewing, the μ are plotted in Fig. 4 as $\text{sgn}(\mu(y)) \log(10|\mu(y)|)$. (These two examples illustrate the general model behavior found for all baroclinically and barotropically unstable modes of the westerly jet.) For the baroclinically unstable mode, the disturbance can propagate between the two critical latitudes (critical latitudes are identified by the large local maxima in μ) but not between the critical latitudes and the walls (the two evanescent regions on either side of the jet vanish for wider jets). On the other hand, for the barotropically unstable mode, three separate propagation regions are found. The interior propagation region is bounded on either side by a turning latitude (turning latitudes are identified as points where $\mu = 0$), whereas the two external propagation regions are bounded by a critical latitude and a turning latitude. In order to communicate between these regions, the disturbance must tunnel through the $\mu < 0$ evanescent region. Thus, both the baroclinically and the barotropically unstable modes are meridionally trapped. The baroclinic mode is trapped between two critical latitudes, whereas the barotropic mode is trapped between two reflecting turning latitudes. As we will see, the difference between the bounding latitudes (i.e., critical latitude vs turning latitude) has important implications for the nonlinear life cycles.

b. Easterly jet

As a representative easterly jet, we first consider the $\sigma = 3.0$ jet with $W = 20.0$. The width of this jet falls within the range of realistic values for the atmosphere. In contrast to the westerly jet, the basic dynamics for the easterly jet is similar for all σ . The marginal stability curve (as with the westerly jet, we take $\omega_i = 0.02$ for the marginal stability curve) for this jet (see Fig. 5)

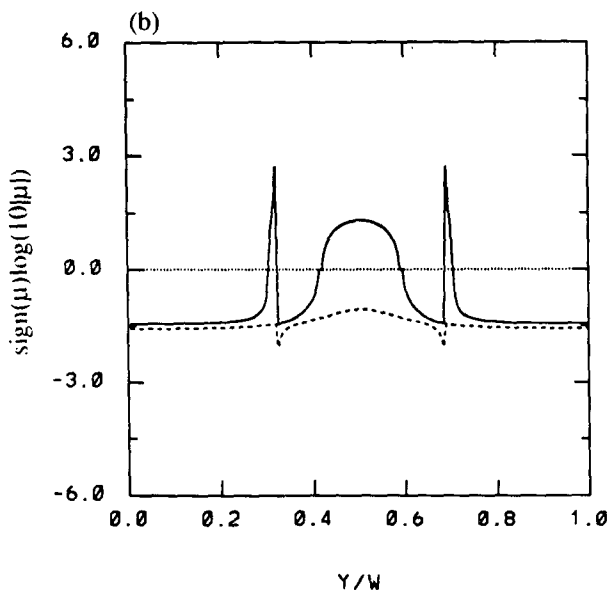
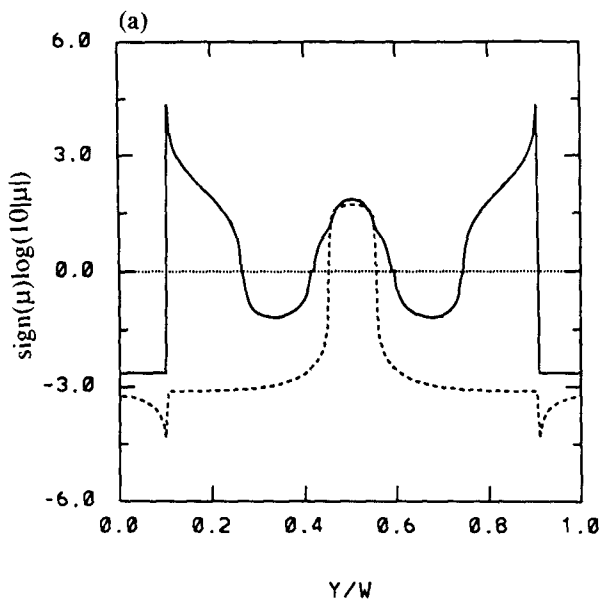


FIG. 4. $\text{Sgn}(\mu) \log(10|\mu|)$ for the $\sigma = 1.0$ westerly jet as a function of y/W for (a) the baroclinically unstable mode with $\beta = 0.42$ and $k = 0.84$, and (b) the barotropically unstable mode with $\beta = 0.361$ and $k = 1.10$.

shows two peaks with $\beta_c = 0.67$ at $k_c = 0.75$ and $\beta_c = 0.685$ at $k_c = 0.95$. These two peaks correspond to the third gravest and the gravest modes, respectively. The zonal wind U_n and the meridional potential vorticity gradient $\partial Q_n / \partial y$ are shown in Fig. 6 for the $\sigma = 3.0$ easterly jet at $\beta = 0.69$. As both horizontal curvature and vertical shear of the zonal flow contribute to the negative $\partial Q_1 / \partial y$ region, it is not found surprising that the unstable modes undergo a combined barotro-

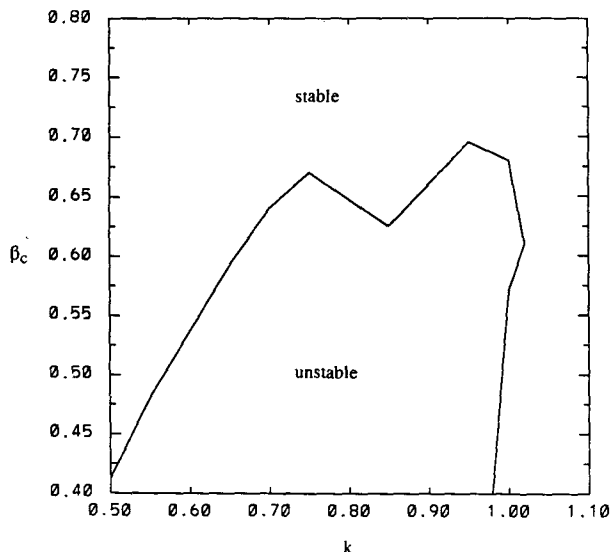


FIG. 5. β_c as a function of zonal wavenumber k for the $\sigma = 3.0$ easterly jet.

pic/baroclinic instability. In addition, for the $\sigma = 3.0$ jet, the baroclinic conversions dominate. Linear stability calculations for other easterly jets find the general trend that as σ decreases both the maximum β_c and the corresponding k_c increase. As an example, for $\sigma = 1.5$, $k_c = 1.47$ and $\beta_c = 1.37$. This systemic behavior is identical to that of the barotropically unstable modes of the narrow westerly jet (width less than the deformation radius), which also show an increase in β_c and

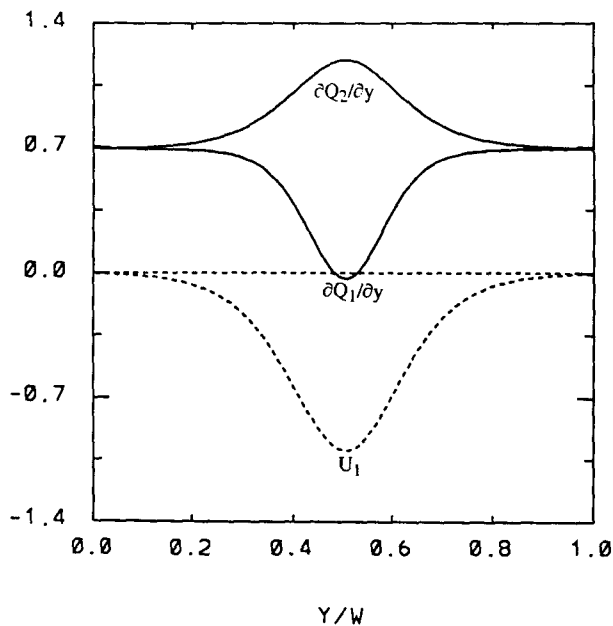


FIG. 6. The initial upper-layer zonal wind U_1 and meridional potential vorticity gradient $\partial Q_n / \partial y$ for the $\sigma = 3.0$ easterly jet with $\beta = 0.69$.

k_c as σ is reduced. The similarity with the barotropically unstable westerly jet is not surprising, since for both types of jets the horizontal curvature of the zonal flow contributes to the upper layer negative $\partial Q_1 / \partial y$ region. A series of linear stability calculations approximately finds for $\sigma > (<) 2.0$ easterly jets that the baroclinic (barotropic) growth is greater than barotropic (baro-

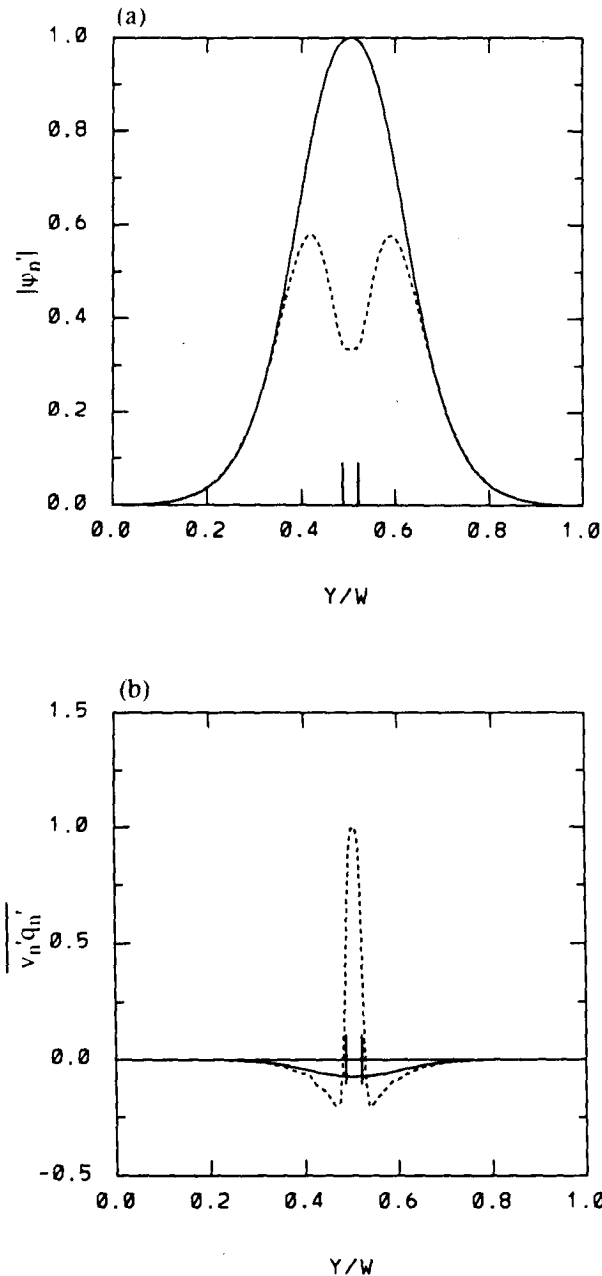


FIG. 7. (a) The magnitude of the streamfunction for the $\sigma = 3.0$ easterly jet unstable mode with $\beta = 0.69$ and $k = 0.95$; and (b) potential vorticity flux for the unstable mode. The solid line corresponds to the lower layer and the dashed line to the upper layer. The streamfunctions and potential vorticity fluxes are normalized by their maximum value.

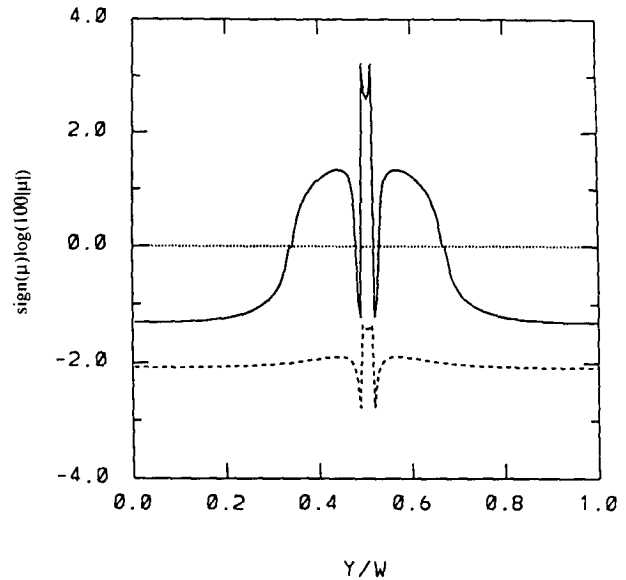


FIG. 8. $\text{Sgn}(\mu) \log(100|\mu|)$ for the $\sigma = 3.0$ easterly jet as a function of y/W for (a) the unstable mode with $\beta = 0.69$ and $k = 0.95$.

clinic) growth. The structure of the $\sigma = 3.0$ linearly unstable mode is illustrated in Fig. 7. For this mode, $k = 0.95$, $\beta = 0.69$, and the growth rate is $\omega_i = 0.02$. In addition, as with the narrow barotropically unstable westerly jets, the critical latitudes are embedded within the negative $\partial Q_n / \partial y$ regions.

A WKB analysis is performed to illustrate the propagation characteristics of marginally stable modes for the easterly jet. Figure 8 shows $\text{sgn}(\mu) \log(100|\mu|)$ as a function of latitude for the $\sigma = 3.0$ case with $\beta = 0.69$. The same behavior is found for other values of σ . By examining the sign of μ , we find an internal propagation region in the center of the channel that is bounded by two turning latitudes. (In the narrow $\mu < 0$ region next to the critical latitude, μ is too small to specify whether the flow is characterized by evanescence.) In some cases (not shown), for small k , the propagation region extends to the walls. Therefore, as in the narrow westerly jet case, the disturbance is trapped and can propagate to and reflect off the external turning latitudes. Thus, the propagation characteristics of the unstable modes of the easterly jet resemble those of the narrow westerly jet (both modes are trapped between turning latitudes) but differ from those of the wider westerly jet that are confined by critical latitudes.

4. Life cycles

In this section, we will investigate the life cycles of disturbances that arise from the instability of both westerly and easterly zonal jets. For these calculations, the initial zonal jet profile is chosen to be weakly supercritical (the supercriticality is defined to be weak when the supercriticality of the initial flow to instability is small enough such that any further reduction of the

supercriticality does not alter the qualitative behavior of the solution). The primary advantage for examining the nonlinear instability of weakly supercritical flows is that the solutions tend to be simpler and much easier to interpret. Typically, when numerical integrations are done at stronger supercriticalities, the solutions become more complicated. Nevertheless, one can often explain aspects of the more complicated strongly supercritical solutions in terms of the simpler weakly supercritical ones.

a. Westerly jet (baroclinic instability)

In this subsection, a series of calculations will be performed to compare the nonlinear evolution of the baroclinically unstable modes growing in jets with different widths. For these calculations, we take $\sigma = 1.0, 3.0, 12.0, 18.0,$ and 24.0 with the same zonal wavenumber $k = 0.82$. For each initial jet profile, the selected value of β corresponds to an initial linear growth rate of $\omega_i = 0.015$ for the disturbance. As σ is increased, the jet width W is set to a larger value to accommodate the wider jet. In addition, because the critical latitude width increases for wider jets [the critical latitude width is proportional to $c_i(\partial U_1/\partial y)^{-1}$ at y_c , and $\partial U_1/\partial y$ at y_c decreases as σ increases], sufficiently accurate solutions can be obtained with coarser resolution at larger σ . Therefore, as calculations are performed for wider jets, we increase the gridpoint spacing (100 grid points in the meridional direction are found to be sufficient) and pick increasingly larger values for ν .

The life cycle solutions for the different values of σ are shown in Fig. 9. As the jet becomes progressively wider, several systematic trends are seen. One is that the time difference between the maximum baroclinic and maximum barotropic energy conversion increases as σ becomes larger. For the $\sigma = 24.0$ jet, the maximum barotropic conversion is delayed so long that the baroclinic conversion has time to change sign, and, as a consequence, the disturbance decays baroclinically.

By examining the upper-layer potential vorticity fluxes, we can obtain a deeper understanding of the dependency of the energy cycles on the jet width (note that the upper layer potential vorticity flux is equal to the difference between the upper layer vorticity flux and heat flux and that at the wings of the jet the heat flux contribution is negligible). Before discussing the key properties of these fluxes, it is necessary to note that the zonal flow is stabilized (i.e., the negative $\partial Q_2/\partial y$ region in the center of the lower layer has been rendered positive) at a time when the upper-layer potential vorticity flux in the center of the channel is very close to its maximum value. Thus, as shown in Fig. 10, we see that the timing of the maximum wave absorption (characterized by the two negative local minima in the potential vorticity flux) relative to that of zonal flow stabilization occurs later for the wider $\sigma = 18.0$ jet. This implies that the timing of the maxi-

imum lateral wave radiation, or equivalently the vorticity flux, shifts to later times as σ is increased. Such behavior is not surprising as the ratio of the linear upper-layer vorticity flux to the linear heat flux decreases as the jet width increases. Therefore, because of the link between the heat (vorticity) flux and the baroclinic (barotropic) energy conversion, this delay in the onset of strong lateral wave radiation for increasingly larger σ can account for the increase in time separation between the maximum baroclinic and barotropic conversions.

The systematic trend in the final zonally averaged flow can be summarized by referring to Figs. 11 and 12. Although only two examples are shown, these results exhibit the general trend in the changes to the zonal flow. For both jets, a similar increase in the U_n is found at the center of the jet, whereas at the wings of the jet the reduction in the U_n for the $\sigma = 6.0$ jet are much more substantial. This difference in the modification to U_n at the wings of the jet can be understood in terms of the weakening of the lateral wave radiation for larger σ . Similarly, a large decrease is seen in $\partial Q_1/\partial y$ at the wings of the $\sigma = 6.0$ jet but not for the $\sigma = 18.0$ jet. In addition, these changes to U_n and $\partial Q_n/\partial y$ occur next to (well before) the critical latitude for the $\sigma = 6.0$ (18.0) jet. The question why some disturbances are absorbed at their critical latitude and others are not (this problem also arises in FH for jets of increasingly larger supercriticalities) is a fundamental one that remains unanswered.

One difference between the two-layer quasi-geostrophic results of FH and those from the spherical multilevel primitive equation model of Simmons and Hoskins (1978) is that Simmons and Hoskins find a greater time difference between the maximum baroclinic and barotropic conversion. [The observation study of Randel and Stanford (1985b) has a time separation that is similar to Simmons and Hoskins.] In FH, where a realistic jet width was used, the barotropic conversion attained its maximum value at a time when the baroclinic conversion decreased by 10%. In the Simmons and Hoskins study, with spherical geometry, the initial barotropic conversions are weak and the maximum barotropic conversion occurs when the baroclinic conversion is reduced by roughly 75%. (In this regard, the time separation between the baroclinic and barotropic conversions for the present $\sigma = 18.0$ jet more closely resembles that seen by Simmons and Hoskins.) This discrepancy can be understood from our examination of the life cycles for different σ . As stated in the previous paragraph, for increasing σ , the linear upper-layer vorticity fluxes are weak and wave radiation is delayed. In addition, for all σ , the vorticity fluxes are positive (negative) in the interior (exterior) of the domain and are symmetric about the center of the channel (this is equivalent to stating that the momentum fluxes converge into the center of the jet). However, in Simmons and Hoskins (1978), the initial

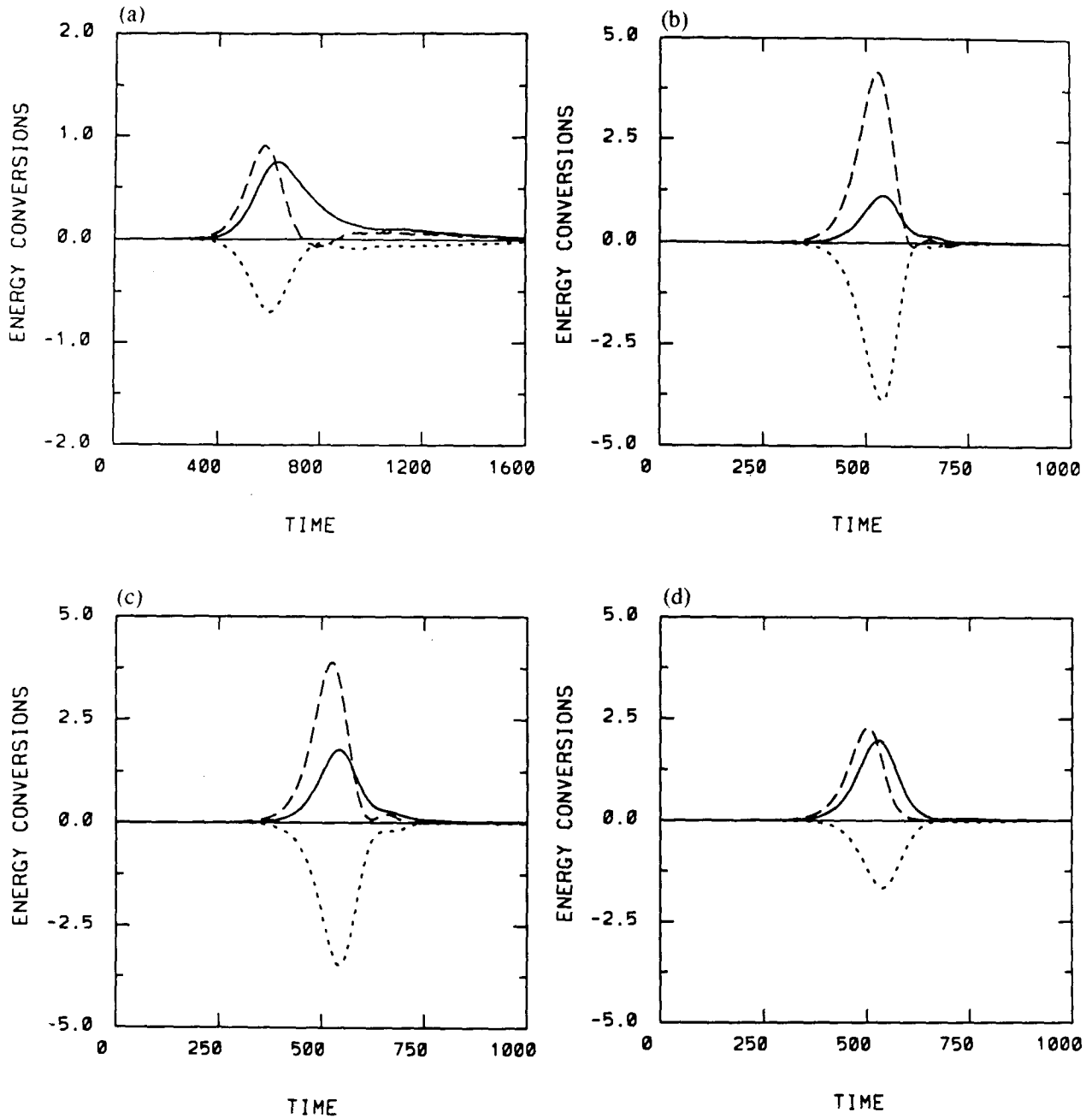


FIG. 9. Eddy energy (multiplied by 2.0×10^3) and energy conversions (multiplied by 1.0×10^5) for the baroclinically unstable westerly jet with (a) $\sigma = 1.0$, $\beta = 0.378$, $W = 7.5$, $\nu = 5.0 \times 10^{-5}$; (b) $\sigma = 3.0$, $\beta = 0.433$, $W = 30.0$, $\nu = 5.0 \times 10^{-5}$; (c) $\sigma = 6.0$, $\beta = 0.466$, $W = 45.0$, $\nu = 5.0 \times 10^{-5}$; (d) $\sigma = 12.0$, $\beta = 0.483$, $W = 90.0$, $\nu = 5.0 \times 10^{-5}$.

momentum fluxes converge at a latitude poleward of the jet maximum. This is because of the spherical geometry of their model. As a result, the initial vorticity fluxes attain their maximum value at a latitude where the zonal wind speed is less than its maximum value. Thus, even though the latitudinal symmetry and scale of the unstable modes for the $\sigma = 18.0$ and the Simmons and Hoskins jet differ, the energetics of the two life cycles resemble each other because of the small

initial barotropic energy conversion. Therefore, the reason that the unstable mode for the $\sigma = 6.0$ jet (also the jet in FH) does not have a realistic time separation between the baroclinic and barotropic conversion is because of the symmetry imposed by the β -plane model.

The above results also indicate that the presence of an absorbing critical latitude in the upper layer is necessary but not sufficient for the existence of a baroclinic

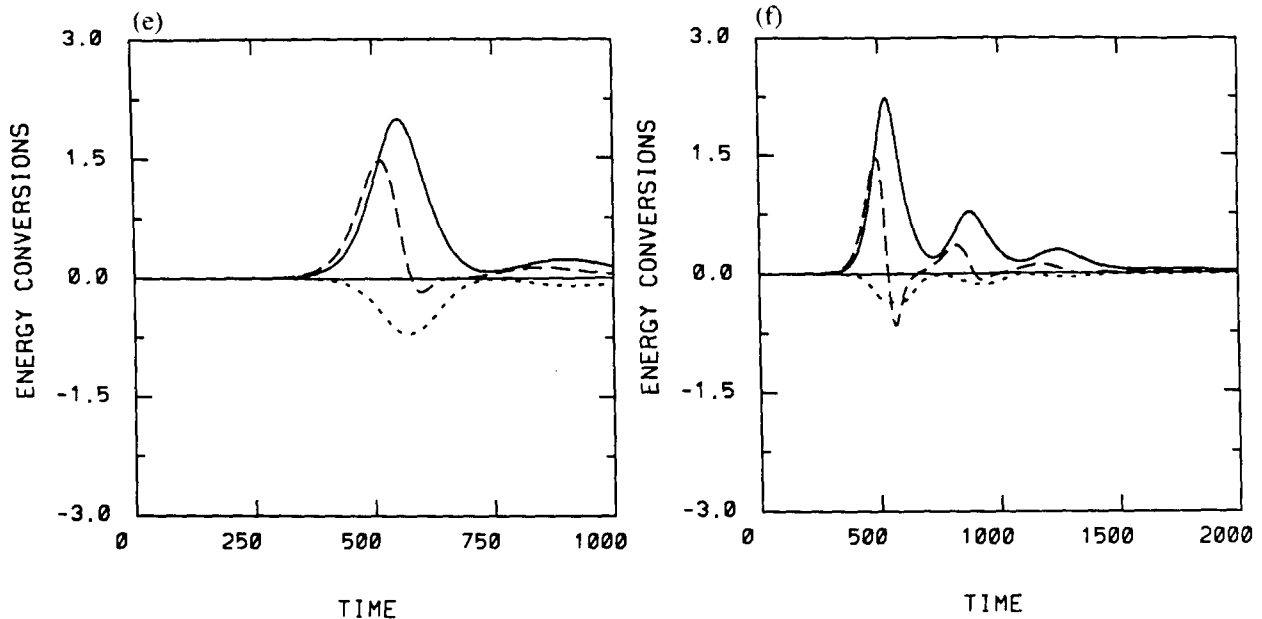


FIG. 9. (Continued) (e) $\sigma = 18.0$, $\beta = 0.489$, $W = 120.0$, $\nu = 1.0 \times 10^{-2}$; and (f) $\sigma = 24.0$, $\beta = 0.491$, $W = 150.0$, $\nu = 1.0 \times 10^{-2}$. Solid line denotes total disturbance energy; long dashed line, baroclinic conversion; short dashed line, barotropic conversion.

growth/barotropic decay life cycle in the two-layer model. We saw one particular example (the $\sigma = 24.0$ jet) where the disturbance grows and decays baroclinically. The barotropic decay was suppressed because significant latitudinal wave radiation did not occur until after the baroclinic conversion changed sign. If we try to extend these results to more realistic models or even to the atmosphere, the above behavior seems to suggest that baroclinic growth/baroclinic decay life cycles are possible if the latitudinal wave radiation is delayed for a long enough period of time.

b. Westerly jet (barotropic instability)

In addition to the above baroclinically unstable modes, we saw that the westerly jet (13) also supports barotropically unstable modes. When the nonlinear barotropic instability calculations are performed, we have to be more careful about horizontal resolution and accuracy at the critical latitude than in the baroclinic problem because of fundamental differences in the role that the critical latitude plays in the two instabilities. In the baroclinic solution, the upper-layer potential vorticity flux attains a significant amplitude at the critical latitude only when the disturbance is radiating latitudinally. The critical latitude acts only as a sink for the disturbance and the detailed structure of the disturbance within the critical latitude is not crucial for an energetic description of the life cycle. In the barotropic problem, the potential vorticity flux at the critical latitude starts out with a relatively large amplitude (see Fig. 3d). Therefore, it is important to re-

solve the disturbance in the critical latitude throughout the entire life cycle. As a result, in contrast to the baroclinic calculation, ν must be chosen to be small enough to be ineffective on the scale of the critical latitude but large enough to dissipate the smallest resolvable length scales.

We next examine the life cycles of the barotropically unstable disturbances. As we saw in the linear stability analysis, barotropically unstable modes occur when σ is less than or equal to order unity. As the general properties of the life cycles of barotropically unstable disturbances are not found to change substantially for different σ (as σ is reduced, the baroclinic conversions are found to be progressively weaker), we will only study the life cycle for the $\sigma = 1.0$ jet. Keeping in mind the above discussion on horizontal resolution, we choose a channel width of $W = 7.5$, use 200 grid points between the channel walls, and select a horizontal diffusion coefficient ν equal to 10^{-9} . In this case, the selection of $k = 1.10$ and $\beta = 0.32$ is made for which the linear growth rate of the disturbance is $\omega_i = 0.03$. When the numerical integrations are performed (see Fig. 13a), the disturbance undergoes a sequence of life cycles consisting of episodes of barotropic growth followed by barotropic decay. Since kinetic energy is returned to the zonal flow once the disturbance starts to decay, further information can be found by examining $\partial Q_n / \partial y$ at the time of maximum disturbance energy (see Fig. 14a). It is apparent, in contrast to that for the baroclinically unstable disturbance, that the disturbance fails to stabilize the zonal flow by removing the negative $\partial Q_1 / \partial y$ region. Furthermore, the temporal

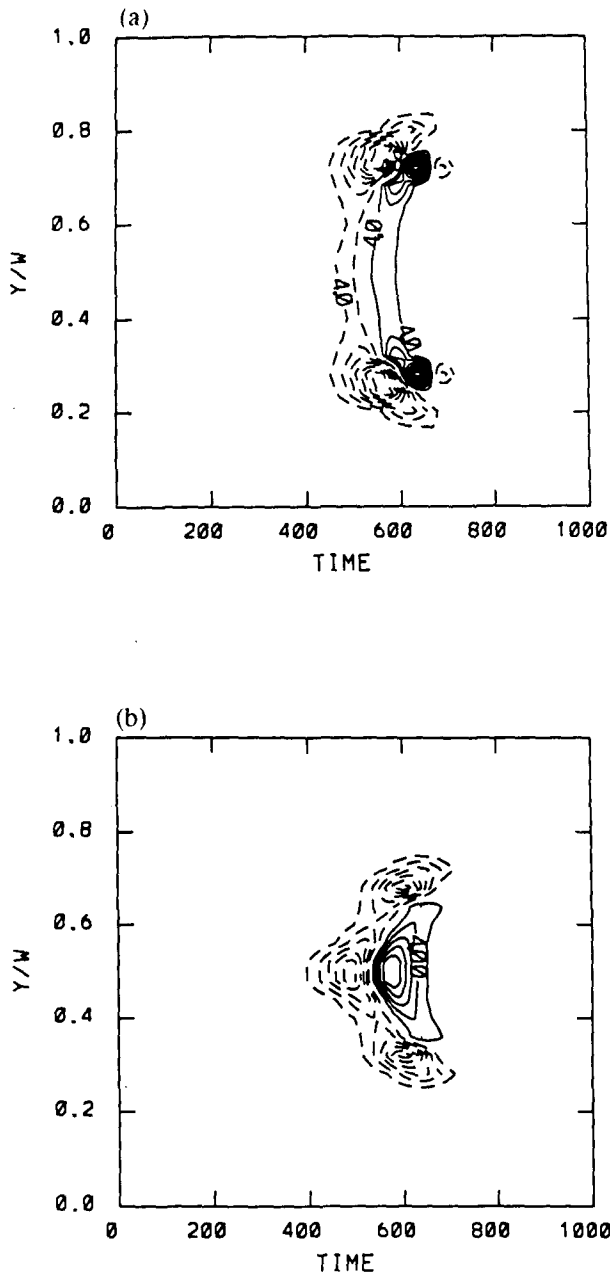


FIG. 10. y/W vs time contour diagram of the potential vorticity flux for the baroclinically unstable westerly jet with (a) the $\sigma = 6.0$ jet, contour interval is 4.0×10^{-5} ; and (b) the $\sigma = 18.0$ jet, contour interval is 2.0×10^{-5} . Solid contours are positive and dashed contours negative.

evolution of the upper-layer potential vorticity flux, shown in Fig. 15a, indicates that the disturbance remains close to its linear normal mode form throughout each cycle. [In the analytical weakly nonlinear theory (e.g., see Pedlosky 1970) for a growing and decaying disturbance, the phase tilt of the lowest-order solution is fixed at a value that corresponds to neutral stability,

whereas at the next highest order the phase oscillates periodically with time. It is this changing phase tilt that is necessary for the disturbance to grow and decay. The above expression "close to its normal mode form" is used in the context of the analytical weakly nonlinear theory to suggest that the disturbance appears to vacillate about its neutrally stable normal mode form.] This contrasts with the life cycle of the baroclinically

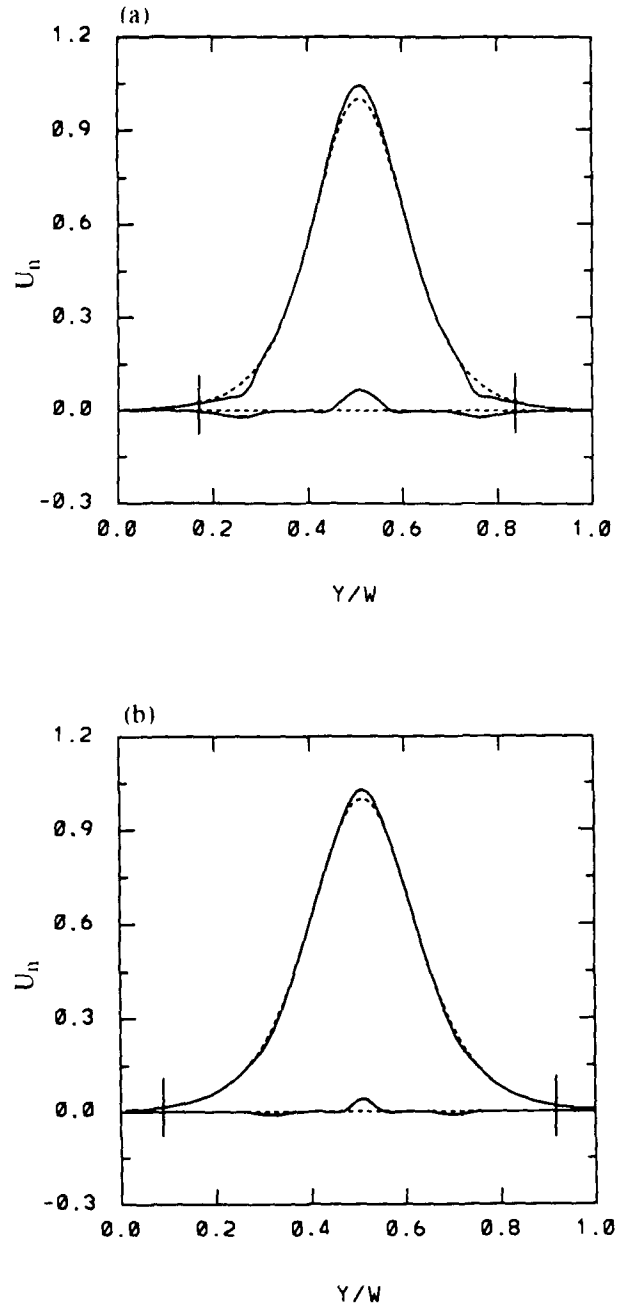


FIG. 11. The initial and final zonal flows U_n for (a) the $\sigma = 6.0$ jet and (b) the $\sigma = 18.0$ jet. Solid line denotes the final zonal flow; dashed line the initial zonal flow.

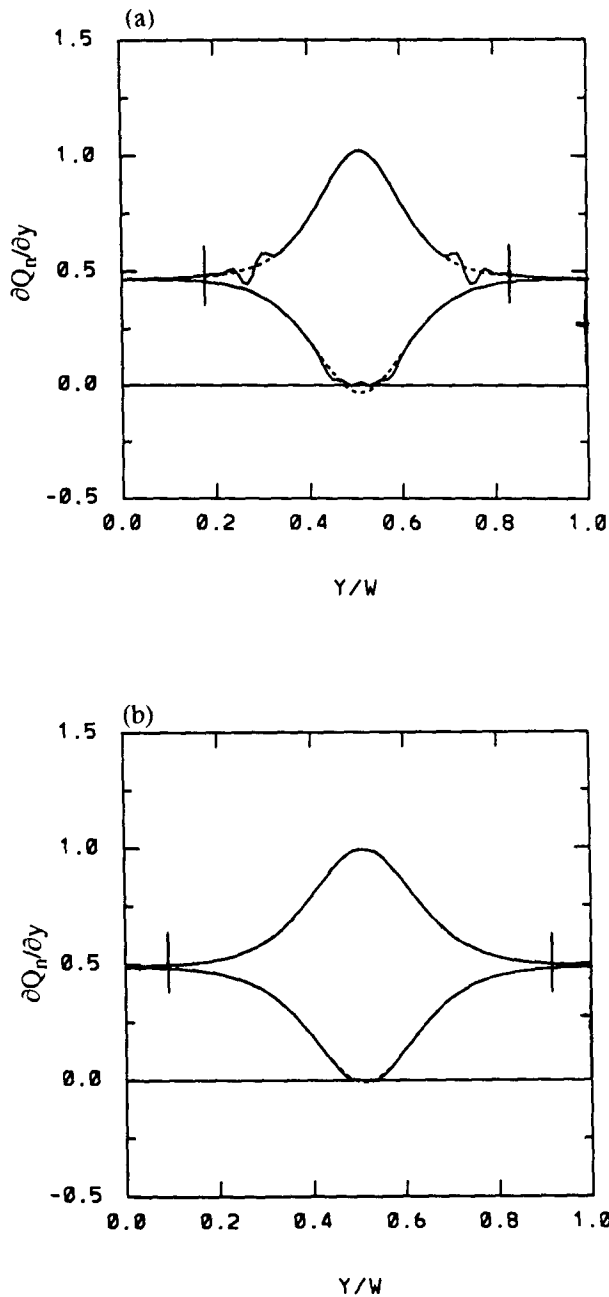


FIG. 12. The initial and final westerly jet meridional potential vorticity gradient $\partial Q_n / \partial y$ for (a) the $\sigma = 6.0$ jet and (b) the $\sigma = 18.0$ jet. Solid line denotes the final zonal flow; dashed line the initial zonal flow.

unstable disturbance that maintains its linear normal mode structure only during the initial growth.

c. Easterly jet

We next investigate the nonlinear evolution of the disturbances arising from the linear instability of the easterly jet. As with the narrow westerly jet, we will

examine in detail the life cycle for just one example, since the general properties of the temporal evolution of the disturbance are found to be the same for all jet widths considered. [The major change found when σ is varied is that narrower (wider) jets are dominated by barotropic (baroclinic) conversions.] As with the narrow westerly jet case, we must be careful about our selection both of the horizontal resolution and the hor-

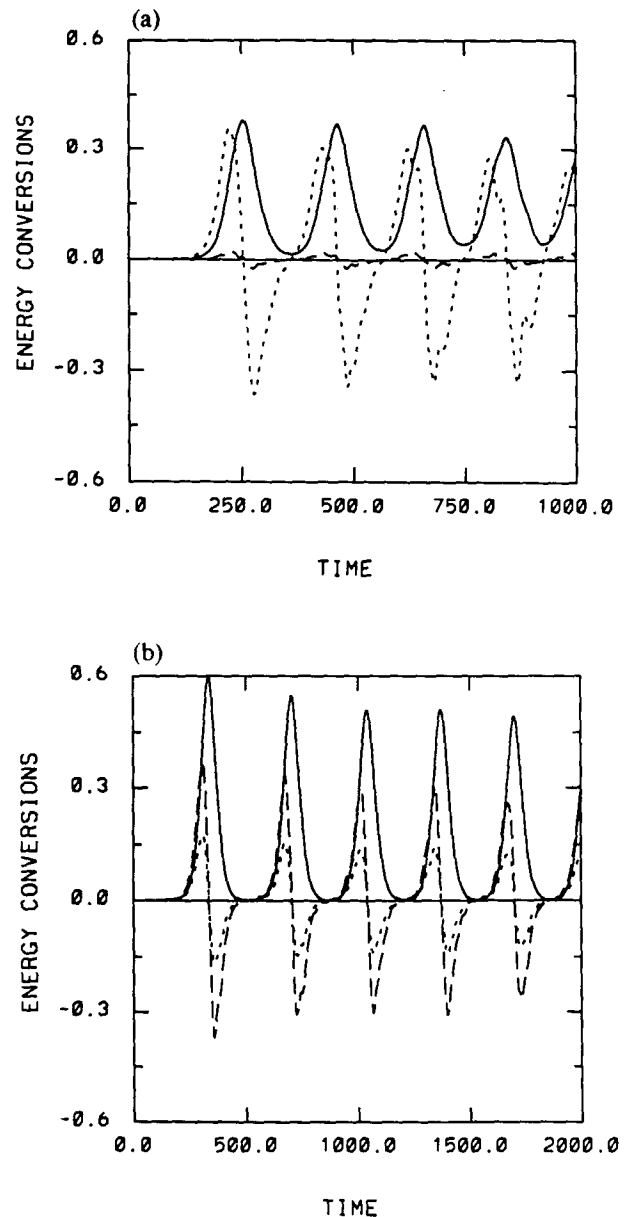


FIG. 13. Eddy energy (multiplied by 2.0×10^3) and energy conversions (multiplied by 1.0×10^5) for (a) the barotropically unstable westerly jet with $\sigma = 1.0$, $\beta = 0.32$, $W = 7.5$, and $\nu = 1.0 \times 10^{-9}$ and (b) the combined baroclinically/barotropically unstable easterly jet with $\sigma = 3.0$, $\beta = 0.67$, $W = 20.0$, and $\nu = 1.0 \times 10^{-9}$. Solid line denotes total disturbance energy; long dashed line, baroclinic conversion; short dashed line, barotropic conversion.

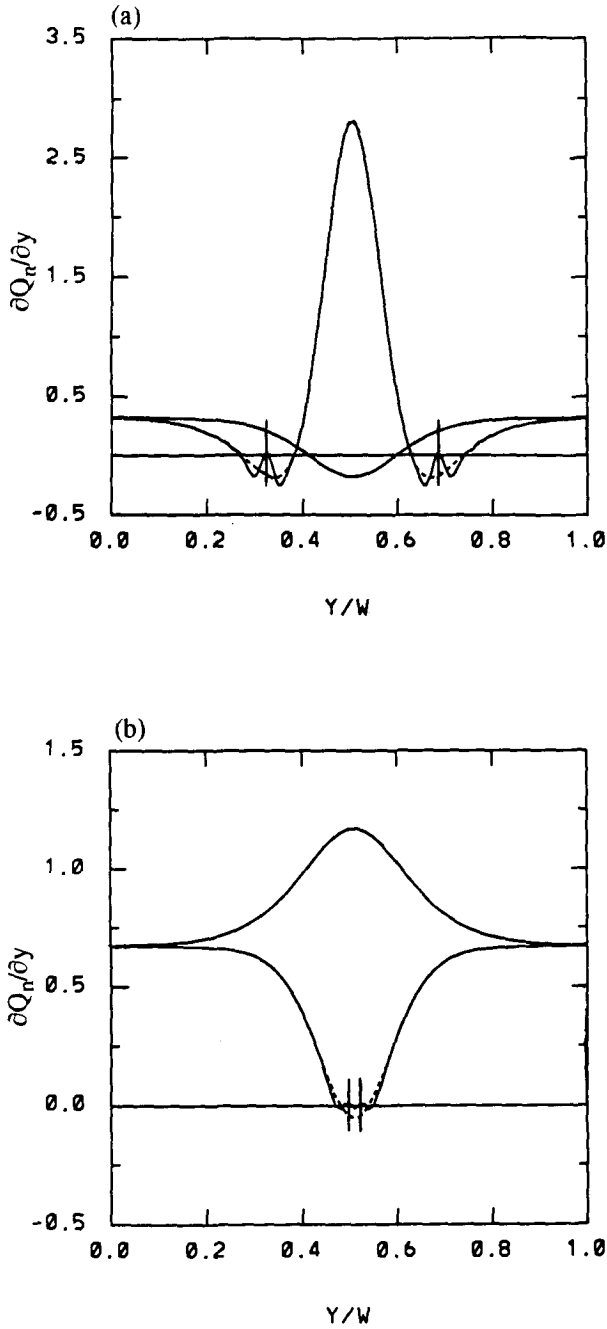


FIG. 14. The meridional potential vorticity gradient $\partial Q_n / \partial y$ both initially and at a time of maximum disturbance total energy (shown at $t = 500$ for both jets) for (a) the $\sigma = 1.0$ barotropically unstable westerly jet and (b) the $\sigma = 3.0$ easterly jet. Solid line denotes $\partial Q_n / \partial y$ ($t = 500$); dashed line $\partial Q_n / \partial y$ ($t = 0$).

horizontal diffusion coefficient ν . We choose $W = 20$, $\nu = 10^{-9}$, and use 200 grid points across the channel. For the present case, we take $\sigma = 3.0$, $k = 0.95$, and $\beta = 0.67$. The linear growth rate of this disturbance is $\omega_i = 0.03$. From our previous linear stability analysis of the easterly jet, we found that the disturbance is trapped

between perfectly reflecting turning latitudes. This closely resembles the narrow westerly jet problem in which the marginally stable modes are also contained by perfectly reflecting surfaces. Because of this similarity, it is not surprising that a series of life cycles (shown in Fig. 13b) is also found. The energetics of these life cycles consist of baroclinic/barotropic growth followed by baroclinic/barotropic decay. In addition,

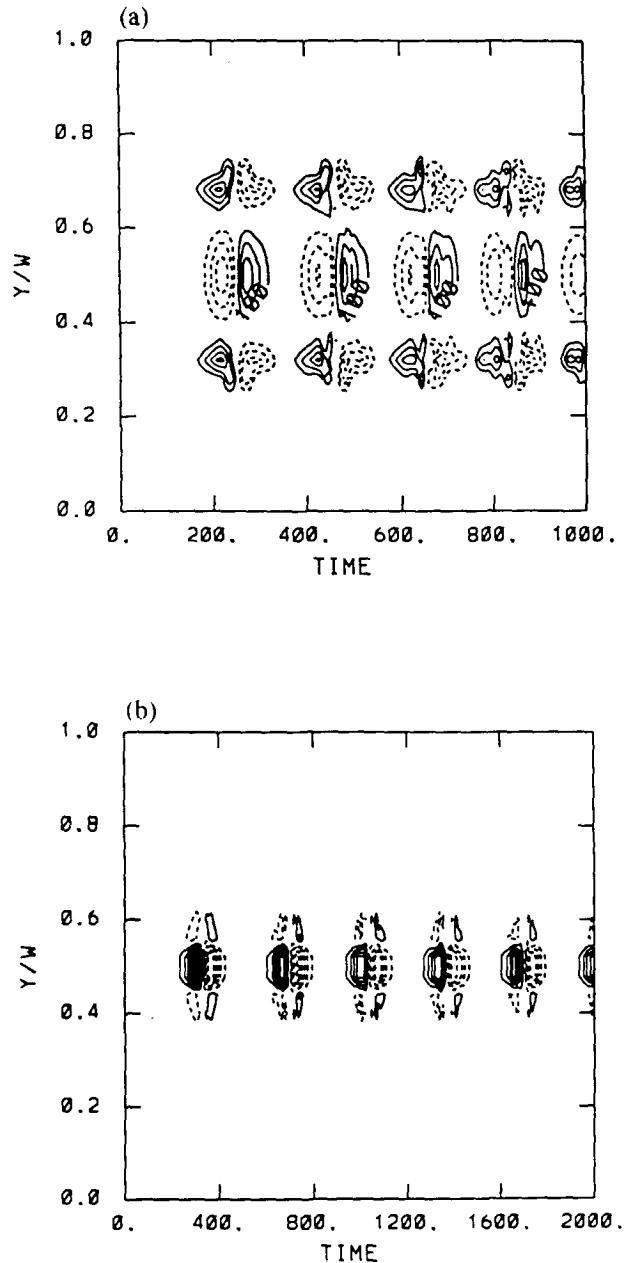


FIG. 15. y/W vs time contour diagram of the potential vorticity flux for (a) the $\sigma = 1.0$ barotropically unstable westerly jet, contour interval is 1.0×10^{-5} ; and (b) the $\sigma = 3.0$ unstable easterly jet, contour interval is 2.0×10^{-5} . Solid contours are positive and dashed contours negative.

as with the narrow westerly jet, $\partial Q_1/\partial y$ at the time of maximum disturbance energy (see Fig. 14b) is still slightly negative so that the zonal flow is not stabilized. Also, as indicated in Fig. 15b, the disturbance stays close to its normal mode structure throughout each episode of growth and decay.

5. Life cycles with forcing and dissipation

In this section, we will investigate the effects of forcing and damping by relaxing the zonal flow back to its initial profile. The disturbance vorticity equation takes on the form

$$\partial q'_n/\partial t + U_n \partial q'_n/\partial x + v'_n \partial Q_n/\partial y = -\nu \nabla^6 \psi'_n - r q'_n, \quad (23)$$

and the zonal mean potential vorticity equation becomes

$$\partial Q_n/\partial t = -\partial(\overline{v'_n q'_n})/\partial y - \nu \nabla^6 \Psi_n - r(Q_n - Q_n^*), \quad (24)$$

where $Q_n(y)^*$ is the potential vorticity of the initial jet profile. The potential vorticity damping in (23) and (24) can be interpreted as physically representing upper- and lower-layer Ekman and thermal damping. The solution with the above forcing and damping for the $\sigma = 6.0$ westerly jet closely resembles those of FH. When r is small, a succession of baroclinic growth/barotropic decay life cycles occurs (see Fig. 14 of FH). As r is increased, this sequence of life cycles is replaced by the evolution of the disturbance amplitude to a steady state. Calculations for other values of σ indicate that all baroclinically unstable modes behave in the same general manner.

We next examine the life cycles that arise from the instability of both the narrow westerly and the easterly jet. For $r = 0$, we saw for both jets that the disturbance undergoes a sequence of life cycles. When (23) and (24) are integrated for any nonzero r (the same initial zonal flows for the calculations in Fig. 13 are used), the disturbance amplitude always evolves to a steady state. (As r decreases, the disturbance takes a longer time to reach a steady state. Because of computational time constraints, this property is verified only for $r \geq 0.001$.) This evolution to a steady state resembles the weakly nonlinear solutions of Pedlosky (1981). He finds steady state solutions in the presence of weak damping in the two-layer quasi-geostrophic β -plane model with a constant zonal flow. Similar behavior is seen by Kwon and Mak (1988), who also find steady solutions for all weakly supercritical, forced, dissipative, zonal flows in their model of the nonlinear barotropic instability of easterly jets. With regard to the energetics of the steady states in the present study, the dominant balance is between barotropic conversions and dissipation for the narrow westerly jet and between the combined baroclinic/barotropic conversion and dissipation for the easterly jet. For both of these jets, the

general behavior remains unchanged for other values of σ .

6. Summary and conclusions

A series of numerical integrations are performed with the two-layer quasi-geostrophic model to compare the nonlinear instability of westerly and easterly jets. In these calculations, the width of both jets is gradually varied. A linear stability analysis first indicates that there are strong asymmetries in the energetics of the unstable modes for the two types of jets. For westerly jets with a width significantly larger (smaller) than the Rossby radius of deformation, a set of larger (smaller) wavelength baroclinically (barotropically) unstable modes are present. Both sets of unstable modes occur when the jet width is close to the deformation radius. This contrasts the easterly jet, which is simultaneously baroclinically and barotropically unstable for all jet widths. The above asymmetries can be traced to the fact that when the jet direction is reversed, the upper layer horizontal wind curvature $\partial^2 U_1/\partial y^2$ changes sign whereas the planetary vorticity gradient β does not.

A WKB solution is obtained for several marginally stable modes of the westerly and easterly jets. The aim of this WKB solution is to determine the regions of wave propagation and evanescence. It is found that the marginally stable modes of the wide westerly jet (width greater than the deformation radius) are confined between two critical latitudes, whereas the marginally stable modes of the narrow westerly (width less than the deformation radius) and easterly jets are trapped between two turning latitudes.

When the nonlinear life cycles are examined, a relationship is found between the linear WKB solution and the nonlinear evolution of the disturbance. This relationship is possible because we are considering the instability of weakly supercritical jets. For disturbances that are confined between two critical latitudes, such as those emanating from the wide westerly jet, a single life cycle of baroclinic growth followed by barotropic decay (the life cycle discussed in FH) occurs. As the width of this jet is increased, the time separation between the maximum baroclinic and barotropic conversion increases. This behavior is related to the delay of the onset of radiation. In addition, for increasingly wider jets, it is found that the strength of the vorticity flux is lessened, which leads to a reduction in the changes to the zonally averaged flow away from the center of the jet. However, the changes in the zonally averaged flow in the center of the jet appear to be only weakly sensitive to the width of the jet. On the other hand, those disturbances that are trapped between turning latitudes undergo a sequence of life cycles. For the narrow westerly (easterly) jet, the disturbance grows and decays in a barotropic (combined barotropic/baroclinic) manner.

The differences in the life cycles of the various jets studied can be related to the characteristics of the

bounding latitudes. For the wide westerly jet, a single life cycle occurs because the disturbance is absorbed either before or at its critical latitude. In addition, because of this absorption, the meridional structure of the disturbance changes with time. In contrast, for both the narrow westerly and easterly jets, multiple life cycles occur because the disturbance is reflected at its turning latitude. Furthermore, consistent with this reflection, the meridional structure of the disturbance is able to remain close to its normal mode form throughout its evolution.

The life cycle solutions for the wide westerly jet resemble those observed in the Southern Hemisphere troposphere (Randel and Stanford 1985b). On the other hand, because zonally symmetric easterly and narrow westerly jets tend to occur in the middle atmosphere, a region of the atmosphere for which there has been a shortage of observation studies (as an example see Randel 1988), one can only speculate about the relationship between the results of the present study and observations. In Lait and Stanford (1988), long-lived planetary waves in the Southern Hemisphere winter stratosphere are observed. This behavior resembles that of the present forced-dissipative narrow westerly jet solutions in the sense that a steady wave state is achieved. The regularity of the observed 2-day wave in the summer mesosphere (see Salby and Roper 1980; Plumb 1983) may also be related to the steadiness found in the forced-dissipative easterly jet solution. Nevertheless, the two-layer model is not sufficient to completely address the relationship between nonlinear instabilities and the persistent middle atmospheric large-scale waves, as numerical models with a more realistic jet and greater vertical and longitudinal resolution are required.

Two important limitations of the present two-layer model, as stated in the previous paragraph, are its vertical and longitudinal resolution. For baroclinically unstable disturbances, the similarity between the two-layer model solution and the life cycles seen in the atmosphere suggests that the two-layer vertical resolution is indeed sufficient. In addition, as shown in FH, the nonlinear evolution of weakly unstable baroclinic disturbances are insensitive to the presence of higher harmonics. However, for the easterly and narrow westerly jets, the vertical and longitudinal resolution are expected, under some circumstances, to be quite important. For instance, if the initial baroclinic conversion is not negligible, the growing disturbance must have a significant vertical component to its EP flux vector. As a result, if this vertically propagating disturbance encounters a reflecting surface such as the ground or a turning level (as was found to occur for horizontal propagation), the life cycles are expected to be qualitatively similar to those found in the two-layer model. On the other hand, if the disturbance meets an absorbing critical level, multiple oscillations to a wave-

free state could be anticipated. In order to assess the sensitivity of the two-layer easterly and narrow westerly jet solutions to longitudinal resolution, a set of preliminary calculations were performed in which four zonal harmonics of the unstable zonal wavenumber were retained. The results from these calculations suggest that for wider versions of the easterly and narrow westerly jets, the disturbance evolution is insensitive to the inclusion of higher harmonics. On the other hand, when the jet width, and in turn the critical latitude width, are reduced, more complicated and irregular life cycles occur. Further studies are being planned to investigate the effects of increased vertical and longitudinal resolution of these life cycles.

Acknowledgments. The computations for this paper were performed on the CRAY X-MP 2/4 supercomputer of the Ontario Center for Large Scale Computation at the University of Toronto. This research was supported by the Atmospheric Environment Service of Canada with a science subvention research grant and by a grant from the Natural Sciences and Engineering Research Council of Canada. I would also like to thank Dr. Isaac Held for his helpful comments on this paper.

REFERENCES

- Boville, B. A., 1980: Amplitude vacillation on an f -plane. *J. Atmos. Sci.*, **37**, 1413-1423.
- , 1981: Amplitude vacillation on a β -plane. *J. Atmos. Sci.*, **38**, 609-618.
- , 1982: Strongly nonlinear vacillation in baroclinic waves. *J. Atmos. Sci.*, **39**, 1227-1240.
- Bretherton, F. P., 1966: Critical layer instability in baroclinic flows. *Quart. J. Roy. Meteor. Soc.*, **92**, 325-334.
- Cai, M., and M. Mak, 1987: Multiplicity of equilibria of baroclinic waves. *Tellus*, **39A**, 116-137.
- Feldstein, S. B., and I. M. Held, 1989: Barotropic decay of baroclinic waves in a two-layer beta-plane model. *J. Atmos. Sci.*, **46**, 3416-3430.
- Hartmann, D. L., 1983: Barotropic instability of the polar night jet stream. *J. Atmos. Sci.*, **40**, 817-835.
- Kwon, H. J., 1989: A reexamination of the genesis of African waves. *J. Atmos. Sci.*, **46**, 3621-3631.
- , and M. Mak, 1988: On the equilibration in nonlinear barotropic instability. *J. Atmos. Sci.*, **45**, 294-308.
- Lait, L. R., and J. L. Stanford, 1988: Fast, long-lived features in the polar stratosphere. *J. Atmos. Sci.*, **45**, 3800-3809.
- Loesch, A. Z., 1974a: Resonant interactions between unstable and neutral baroclinic waves, part 1. *J. Atmos. Sci.*, **31**, 1177-1201.
- , 1974b: Resonant interactions between unstable and neutral baroclinic waves, part 2. *J. Atmos. Sci.*, **31**, 1202-1217.
- Mak, M., 1985: Equilibration in nonlinear baroclinic instability. *J. Atmos. Sci.*, **42**, 2764-2782.
- Manney, G. L., T. R. Nathan and J. L. Stanford, 1988: Barotropic instability of realistic stratosphere jets. *J. Atmos. Sci.*, **45**, 2545-2555.
- Mass, C., 1979: A linear primitive equation model of African wave disturbances. *J. Atmos. Sci.*, **36**, 2075-2092.
- Mishra, S. K., and M. K. Tandon, 1983: A combined barotropic-baroclinic instability study of the upper tropospheric tropical easterly jet. *J. Atmos. Sci.*, **40**, 2708-2723.

- Pedlosky, J., 1970: Finite-amplitude baroclinic waves. *J. Atmos. Sci.*, **27**, 15–30.
- , 1971: Finite-amplitude baroclinic waves with small dissipation. *J. Atmos. Sci.*, **28**, 587–597.
- , 1981: The effect of β on the chaotic behavior of unstable baroclinic waves. *J. Atmos. Sci.*, **38**, 717–731.
- , 1987: *Geophysical Fluid Dynamics*, 2nd ed., Springer-Verlag, 710 pp.
- , and C. Frenzen, 1980: Chaotic and periodic behavior of finite-amplitude baroclinic waves. *J. Atmos. Sci.*, **37**, 1177–1196.
- Pfister, L., 1979: A theoretical study of three-dimensional barotropic instability with applications to the upper stratosphere. *J. Atmos. Sci.*, **36**, 908–920.
- , 1985: Baroclinic instability of easterly jets with applications to the summer mesosphere. *J. Atmos. Sci.*, **42**, 313–330.
- Plumb, R. A., 1983: Baroclinic instability of the summer mesosphere: A mechanism for the quasi-two-day wave? *J. Atmos. Sci.*, **40**, 262–270.
- Randel, W. J., 1988: The seasonal evolution of planetary waves in the Southern Hemisphere stratosphere and troposphere. *Quart. J. Roy. Meteor. Soc.*, **114**, 1385–1409.
- , and J. L. Stanford, 1985a: An observational study of medium-scale wave dynamics in the Southern Hemisphere summer. Part I: Wave structure and energetics. *J. Atmos. Sci.*, **42**, 1172–1188.
- , and ———, 1985b: The observed life cycle of a baroclinic instability. *J. Atmos. Sci.*, **35**, 1364–1373.
- Rennick, M. A., 1976: The generation of African waves. *J. Atmos. Sci.*, **33**, 1955–1969.
- Salby, M. L., and R. G. Roper, 1980: Long period oscillations in the meteor region. *J. Atmos. Sci.*, **37**, 237–244.
- Simmons, A. J., 1977: Baroclinic instability in the summer mesosphere. *Quart. J. Roy. Meteor. Soc.*, **103**, 211–214.
- , and B. J. Hoskins, 1978: The life cycles of some nonlinear baroclinic waves. *J. Atmos. Sci.*, **35**, 414–432.
- , and ———, 1980: Barotropic influences on the growth and decay of non-linear baroclinic waves. *J. Atmos. Sci.*, **37**, 1679–1684.